

## Mechanisms of fast-ice development in the south-eastern Laptev Sea: a case study for winter of 2007/08 and 2009/10

Valeria Selyuzhenok <sup>a,c,e</sup>, Andrew Mahoney<sup>b</sup>, Thomas Krumpen<sup>c</sup>, Giulia Castellani<sup>d</sup> & Rüdiger Gerdes<sup>c</sup>

<sup>a</sup>Climate Variability and Change in High Northern Latitudes, Nansen International Environmental and Remote Sensing Centre, St Petersburg, Russia; <sup>b</sup>Geophysical Institute, University of Alaska Fairbanks, University of Alaska, Fairbanks, AK, USA; <sup>c</sup>Sea Ice Physics, Alfred Wegener Institute Helmholtz-Zentrum für Polar- und Meeresforschung, Bremerhaven, Germany; <sup>d</sup>Polar Biological Oceanography, Alfred Wegener Institute Helmholtz-Zentrum für Polar- und Meeresforschung, Bremerhaven, Germany; <sup>e</sup>Department of Cartography & Geoinformatics of the Institute of Earth Sciences, St Petersburg State University, St Petersburg, Russia

### ABSTRACT

Accurate representation of fast ice in numerical models is important for realistic simulation of numerous sea-ice and ocean variables. In order to simulate seasonal and interannual variability of fast-ice extent, the mechanisms controlling fast-ice development need to be thoroughly understood. The objective of this paper is to investigate mechanisms contributing to the advance of fast-ice edge to its winter location in the south-eastern Laptev Sea. The study is based on time series of synthetic aperture radar (SAR) imagery for winter 2007/08 and 2009/10. A detailed examination of SAR-based ice drift showed that several grounded ice features are formed offshore prior to fast-ice expansion. These features play a key role in offshore advance of the fast-ice edge and serve as stabilizing points for surrounding pack ice as it becomes landfast. Electromagnetic ice thickness measurements suggest that the grounded ice ridges over water depths of ca. 20 m water might be responsible for interannual variations in fast-ice edge position. Contrary to previous studies, we conclude that grounding is a key mechanism of fast-ice development in the south-eastern Laptev Sea.

### KEYWORDS

Landfast ice; stamukha; SAR; EM sea-ice thickness; Lagrangian drift

### ABBREVIATIONS

EM: electromagnetic; ENVISAT: Environmental Satellite; GDSIDB: Global Digital Sea Ice Data Bank, maintained by the World Meteorological Organization and the Arctic and Antarctic Research Institute (St. Petersburg); IPS: upward-looking ice-profiling sonar; SAR: synthetic aperture radar

Fast ice is a dominant sea-ice feature of the Arctic coastal region. Accurate representation of fast ice is found to be important for realistic simulations of Arctic sea-ice concentration and thickness (Jakobsson et al. 2012), ocean height (Proshutinsky et al. 2007), Arctic halocline stability (Itkin et al. 2015) and upwelling of North Atlantic water (Pickart et al. 2011). The majority of today's coupled sea-ice–ocean models are not capable of representing seasonal variability of fast-ice extent. To improve ice–ocean models and successfully incorporate fast ice, the mechanisms controlling seasonal fast-ice development need to be further explored and thoroughly understood.

The lateral extent of fast ice as well as the mechanisms controlling it differs on a regional scale. In the Kara Sea, fast ice forms between a chain of islands and the mainland, extending up to 300 km offshore over waters deeper than 100 m (Divine et al. 2004; Olason 2016). The interannual variability of Kara Sea fast-ice extent is linked to the prevailing atmospheric circulation patterns (Divine et al. 2005). A narrower 5–50 km fast-ice band forms along the Alaska coast in the Chukchi and Beaufort seas. There, the typical

winter fast-ice extent appears to be controlled largely by a system of grounded pressure ridges, which stabilize the fast-ice edge at depths of around 20 m (Reimnitz et al. 1994; Mahoney et al. 2007). The presence of grounded ice island and tabular icebergs leads to the formation of extensive fast-ice cover north-east of Greenland (Hughes et al. 2011). The Laptev Sea and East Siberian Sea are characterized by the broadest fast-ice extent in the Arctic. Because of geographical similarity of the two regions, the East Siberian Sea and Laptev Sea fast-ice covers are considered to have similar characteristics (Timokhov 1994); however, there is no comprehensive study of the East Siberian fast ice. In the south-eastern Laptev Sea, the fast-ice edge advances to 20–25 m water depth (Selyuzhenok et al. 2015). However, the processes leading to the development of up to 500 km-wide fast-ice cover in the south-eastern Laptev Sea are not well-understood. According to previous studies (Reimnitz et al. 1994; Eicken et al. 2005), the lack of ridges of significant height along the fast-ice edge indicates that the extent of fast ice is not directly controlled by ice deformation and the grounding position of the deepest pressure ridge keels.

**CONTACT** Valeria Selyuzhenok  [valeria.selyuzhenok@niersc.spb.ru](mailto:valeria.selyuzhenok@niersc.spb.ru), 14 liniya V.O. 7, St Petersburg 199034, Russia

 Supplementary material for this article can be accessed [here](#).

© 2017 The Author(s). Published by Informa UK Limited, trading as Taylor & Francis Group.

This is an Open Access article distributed under the terms of the Creative Commons Attribution-NonCommercial License (<http://creativecommons.org/licenses/by-nc/4.0/>), which permits unrestricted non-commercial use, distribution, and reproduction in any medium, provided the original work is properly cited.

In the south-eastern Laptev Sea the annual fast-ice cycle begins with a gradual advance of the fast-ice edge to water depths around 10 m. This is typically followed by a series of rapid development events, which advance fast-ice edge to its maximum winter location, which it occupies from February to July. From the lack of deformed ice, Eicken et al. (2005) concluded that fast ice in the Laptev Sea develops via a gradual accretion of ice floes, while Karklin et al. (2013) suggested that a shift in atmospheric circulation from offshore to onshore wind triggers rapid fast-ice development. Based on a 14-year time series from operational sea-ice charts, Selyuzhenok et al. (2015) suggested that the time required for fast ice in the Laptev Sea to reach its maximum winter extent depends on the growth rate of the sea-ice thickness. However, the accuracy and temporal resolution of fast-ice data used by Selyuzhenok et al. (2015) did not allow a conclusive analysis of any linkage to the direction of cross-shore winds.

In this paper, we investigate more closely the mechanisms contributing to the advance of fast-ice edge to its winter location in the south-eastern Laptev Sea through a combination of high-resolution satellite and observational data. Using time series of SAR images, we track the development of fast ice in the winters of 2007/08 and 2009/10. Then we analyse patterns of fast-ice development and wind conditions in the two seasons. Last, the sea-ice thickness measurements are used to discuss the role of ice ridging in the development of fast ice in the region.

## Methods

### Drift detection and classification

We used a time series of geolocated ENVISAT C-band SAR images to follow the development of fast ice in the 2007/08 and 2009/10 winter seasons. For each season the investigation started on an arbitrary date in the fall, when most of the area was covered with pack ice, and ends once the SAR images indicated the presence of a fast-ice cover that is close to its winter extent (ca.  $130 \cdot 10^3 \text{ km}^2$ ). The areal development of fast ice during the investigation period is shown in Fig. 1.

Overall, we obtained 21 SAR scenes between 3 December 2007 and 23 January 2008 and 10 scenes between 1 December 2009 and 15 February 2010. The images have a pixel resolution of 150 m. The time interval between acquisitions varied between 10 hours and four days for the 2007/08 season, and between three and 14 days for the 2009/10 season. The spatial coverage of the SAR data is shown in Fig. 2.

Using the Environment for Visualizing Images tool (Harris Geospatial Solutions) we derived

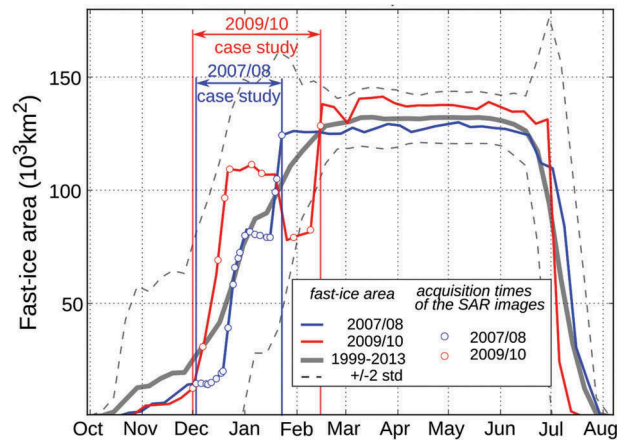


**Figure 1.** Annual development of fast-ice area in the south-eastern Laptev Sea ( $71\text{--}77^{\circ}\text{N}/125\text{--}139^{\circ}\text{E}$ ), derived from GDSIDB operational sea-ice charts (WMO 2016). The grey curves show mean fast-ice area (thick line) and two standard deviations (dashed line) calculated for 1999–2013 (from Selyuzhenok et al. 2015). The blue and red curves show the fast-ice areas in 2007/08 and 2009/10, respectively, and the vertical lines indicate the periods of investigation.

Lagrangian drift of sea-ice features in the area by manually tracking the features on consecutive images. The features were selected such that they were well distributed over the whole area and had recognizable backscatter patterns to allow for feature tracking. In the course of investigation some features were lost as a result of sea-ice deformation. In such cases, we identified a new feature in the vicinity of the lost one and the lost feature was removed from subsequent analysis. As a result of sea-ice deformation and spatially irregular SAR-coverage, the number of times each feature was observed is not constant. Hence, for the final analysis we selected features with three or more observations. Overall, we selected 31 features in 2007/08 and 37 features in 2009/10. Their initial locations are shown in Fig. 2.

For each sea-ice feature we calculated a time series of the drift speed (Supplementary Figs. S1, S2) based on the feature displacement and the time interval between the SAR scenes. Assuming that image geolocation error does not exceed one pixel and the position errors of manual feature selection is less than three pixels, we estimate the overall error of the tracking approach to not exceed 600 m. The corresponding error of drift estimates ranges from  $0.05 \text{ cm}\cdot\text{s}^{-1}$  to  $1.7 \text{ cm}\cdot\text{s}^{-1}$  depending on the time span between image pairs.

Next, each feature was attributed with a date when it was incorporated into fast ice. This date was defined as the first date on which a feature was observed at a location that it subsequently occupied for at least one week without moving (detected drift speed of a feature is less than the corresponding error of drift estimate). In the event of a non-zero drift

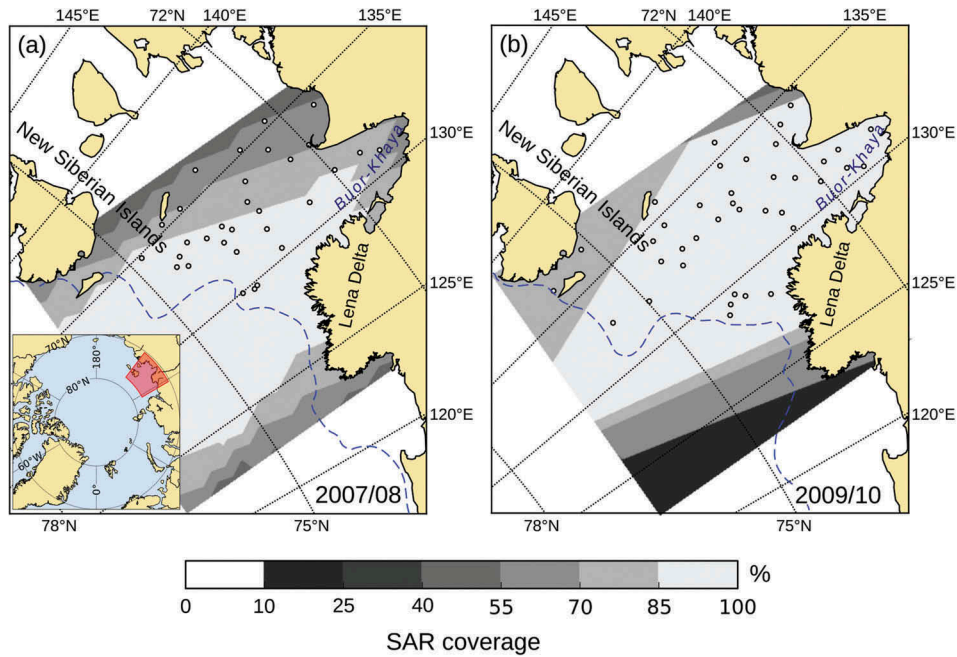


**Figure 2.** Study area and SAR coverage. The grey colour corresponds to a fraction of SAR scenes obtained over the area of interest. The initial position of the tracked sea-ice features is shown in circles. The dashed blue line shows the position of the fast-ice edge on (a) 23 January 2008 and (b) 16 February 2010, taken from GDSIDB operational sea-ice charts (WMO 2016).

measurement after that date (features 29–31 in 2007/08 and 32–38 in 2009/10), it was marked as a break-out.

The accuracy with which it is possible to determine the fast-ice incorporation date depends on the number of observations and therefore is different for every fast-ice feature. To reduce the biases we classify the features in four fast-ice groups (Group I–IV) according to the date when a feature was classified as fast ice. Group I includes the features that were immobile already on the first image pair and therefore classified as fast ice on the first day of the investigation period. The rest of investigation period was split into three equal intervals (Fig. 3a, c). Groups II–IV comprise features that were incorporated into the fast ice during a corresponding time interval. Note that the intervals are different for each season.

### Auxiliary data

#### Wind data

To examine the role of wind action during the course of fast-ice development we used 6-hour ERA-Interim reanalysis wind data extracted from a position located in the centre of the area of interest (75°N/133.5°E). These data were used to derive the distribution of wind speed in different directions for two seasons (Fig. 3). To facilitate the comparison of wind and drift directions, we define wind direction as the direction the wind is blowing to. Hence, northward wind corresponds to the offshore wind blowing to the north.

### Sea-ice draft and keels information

The main information on sea-ice ridging was derived from helicopter-borne EM measurements taken on 29 April 2008. Since no other extensive fast-ice thickness measurement was performed during the period of investigation, we use an additional EM ice-thickness data set obtained during 16–20 April 2012 and upward-looking sonar data obtained in November–February 2013.

The aim of the 2008 campaign was to estimate ice production over polynyas, hence, only a little fast-ice area was covered. In fact, fast-ice measurements are limited to areas close to the fast-ice edge. In 2012 however, extensive flights over fast-ice areas located further inshore were made. Because the EM ice thickness can be significantly overestimated in shallow waters, both profiles were made over the water depth greater than 10 m (Hendricks et al. 2014).

For both profiles, sea-ice thickness and sea-ice surface elevation were derived using an electromagnetic-induction system (EM-bird) and a Riegel LD90-3100HS laser altimeter (Haas et al. 2009). The EM sea-ice thickness has an average point spacing of 4 m and a footprint of 40–50 m. The accuracy of level-ice thickness estimates within a footprint is approximately 10 cm (Pfaffling et al. 2007; Haas et al. 2009). The point spacing of the laser altimetry data is 30–40 cm and the accuracy is within 1.5 cm. A combination of a low and high pass filter was applied to the altimeter data to remove the variations of the surface elevation resulting from the helicopter movement (Hibler 1972).

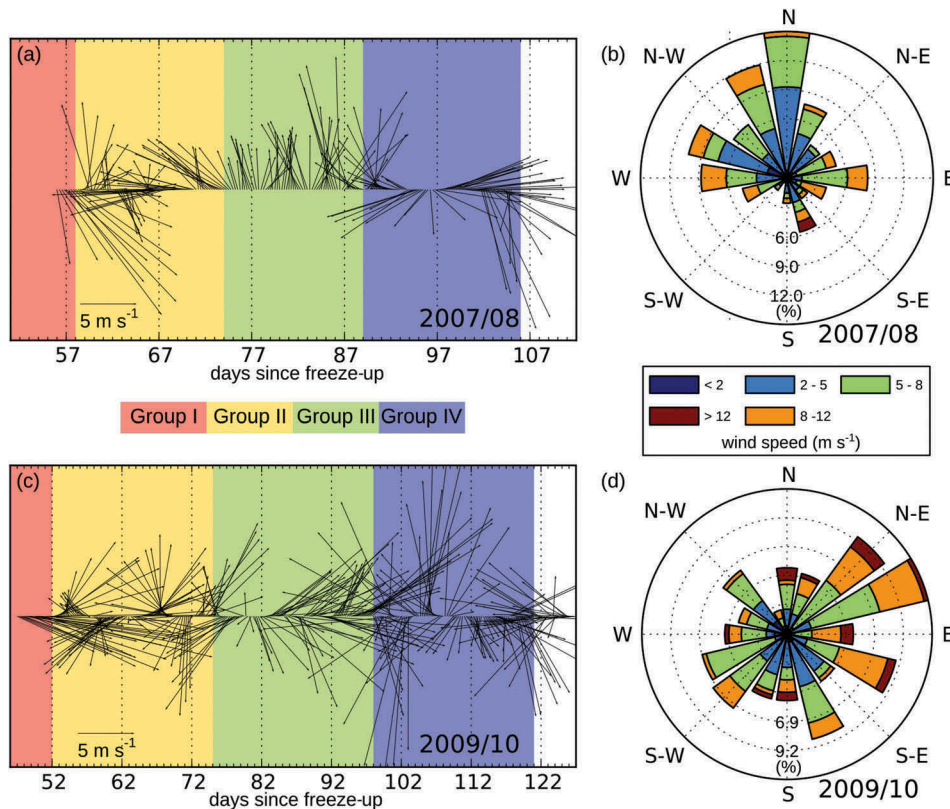


**Figure 3.** Wind speed and direction at the location 75°N/133.5°E for two seasons: 2007/08 and 2009/10. (a, c) Time series of wind vectors and (b, d) the corresponding wind rose. In (a) and (c), the background colour corresponds to fast-ice groups (Group I-IV) and indicates time intervals of fast-ice formation for a corresponding group. In (b) and (d), the sign convention is that the northward wind direction corresponds to the bar directed to the north.

Following Castellani et al. (2015), we identified the sea-ice ridges along the profiles from EM and laser altimeter measurements. First, the sea-ice bottom topography was derived as a difference of the surface elevation and EM ice thickness for each point where both measurements are available. The minima in the bottom topography deeper than 1.5 m were identified as keel bottoms. Two adjacent keels were classified as separate features if they satisfied the Rayleigh criterion: the minimum point between two separate keels must be separated by a point whose depth is less than half of the maximum depth of the keel (Hibler 1975; Wadhams & Davy 1986). Because of a large footprint and the presence of seawater in the keel's cavities, the EM method underestimates the real-ridge thickness by 40–80% (Reid et al. 2003; Haas 2004; Hendricks 2009). Taking into account the typical underestimation of 50% (Pfaffhuber et al. 2012), the maximum depths of detected keels were multiplied by a factor of two in order to account for the systematic underestimation of the EM method (Haas 2004).

Additional information on fall sea-ice draft thickness in the Laptev Sea was collected at two seafloor observatories. In September 2013, two Ice Profiling Sonars (version 5), manufactured by ASL Environmental Science Inc., and two Acoustic Doppler Current Profilers were deployed in the

Laptev Sea at mooring locations 1893 (76°N/126°E at 25 m instrument depth) and Taymyr (77.25°N/116°E at 24 m instrument depth). These systems were sampling the distance to ice surface at an interval of 1 second between October and July and recovered in September 2014. The measured parameters – sound pulse travel time, instrument tilt, temperature and pressure – were converted by ASL into ice draft following their standard processing routines (Melling et al. 1995). Based on the accuracy and precision of the acoustic, pressure, tilt and temperature sensor of the IPS, the error of the obtained draft thickness is within  $\pm 0.05$  m.

## Results

### *Sea-ice and wind conditions in 2007/08 and 2009/10*

According to GDSIDB operational maps (WMO 2016), the development of fast-ice area in 2007/08 closely followed the 1999–2013 average areal development (Fig. 1) and is representative for the majority of seasons. In comparison to 2007/08, the winter of 2009/10 was characterized by an unusual break-out event in January–February (Fig. 1). The initial sea-ice conditions at the beginning of investigation for the two seasons were slightly different. According to a

passive-microwave data set (Markus et al. 2009), the freeze-up in 2007/08 occurred on 6 October. The first analysed SAR scene was taken 58 days after the freeze-up. It showed that the area of interest was almost entirely covered with pack ice (nearly 100% concentration). A small patch (ca.  $3 \cdot 10^3 \text{ km}^2$ ) of newly-formed ice along the east Lena Delta developed during a coastal polynya event. A significantly bigger area ( $> 21 \cdot 10^3 \text{ km}^2$ ) of newly formed ice was present along the Lena Delta on the first SAR scene (taken 52 days after freeze-up) in 2009/10. Freeze-up in 2009/10 took place seven days later than in 2007/08.

The two seasons were also characterized by different wind conditions. In general, the wind circulation in the Laptev Sea can be described by two main regimes: an anticyclonic regime with a dominant northward (offshore) component and a cyclonic regime with a dominant north-eastward component (wind towards the East Siberian Sea) (Dmitrenko et al. 2005). In 2007/08 north-, west- and north-westward wind with an average speed of  $5\text{--}8 \text{ m s}^{-1}$  was predominant (Fig. 3b). Remarkably, the offshore wind (in north-west–north direction) persisted for two weeks (days 71–86 in (Fig. 3a)). The season 2009/10 was characterized by slightly higher wind speeds (Fig. 3c) and more scattered directions. The predominant wind direction for that season was north-east–east (Fig. 3d). The beginning of a period of strong wind speed (up to  $26 \text{ m s}^{-1}$ ) in north and north-east direction between day 103 and day 110 (Fig. 3c) coincided with the timing of fast-ice break-up that was observed in January–February between days 90 and 119. Overall, the season 2007/08 was characterized by stronger offshore wind component (anticyclonic regime) and the season 2009/10 shows stronger eastward wind component (cyclonic regime).

### Fast-ice development based on drift classification

Figure 4 shows the time series of mean drift speed for the four fast-ice groups (Groups I–IV). By definition, Group I showed zero drift speed from the beginning of the investigation. Groups II–IV were characterized by higher drift speed at the beginning of the investigation period; this speed decreased towards the end.

In 2007/08 the drift speed for Groups II–IV was relatively high between days 55 – 65 and dropped after day 65 to  $1\text{--}2 \text{ m s}^{-1}$ . Afterwards, the drift speed decreased gradually. Only Group IV showed a slight peak in the drift speed towards the end of the investigation.

In 2009/10 only Group I features were tracked from the beginning of the investigation. As a result of deformation of the vast thin ice zone formed during a polynya event and covering a substantial part of the area of interest, many features were lost at the beginning of the investigation period. This resulted in shorter drift time series of Group II–IV. The pattern of Group II–IV drift speed, however, looks similar to the one in 2007/08: there was a drop in drift speed followed by a gradual decline in velocity to zero motion. This indicates that the formation of fast ice in both seasons did not occur abruptly, but was a gradual process of ice flow accretion, as suggested by Eicken et al. (2005).

The final location of all tracked features is shown in Fig. 5. In both seasons, Group I features are located not only in the vicinity ( $< 50 \text{ km}$ ) of the shore, where fast ice is typically expected to start forming, but also further offshore, surrounded by mobile pack ice. The location of these offshore features corresponds to the shallow banks, suggesting that the ice was grounded there. The mean water depth at the location of Group I features was  $10 \text{ m}$  (Fig. 6). Notably, the Group I features re-occurred at the same location in both seasons. The location of Group II and III features does not show any spatial pattern. Features that remained mobile until the latter third of each investigation period (Group IV) occupied the deepest waters (Fig. 6) and were found in two different regions (Fig. 5). Most were observed in the seaward most portion of fast ice, which is typically last to stabilize. However, a number of features were observed to continue drifting with low speed near the mouth of the Buor-Khaya Bight despite being surrounded by stationary fast ice.

During the course of fast-ice formation some of the features (Fig. 5) were incorporated in fast ice, but later became mobile again. These events were classified as break-out events. In 2007/08 break-

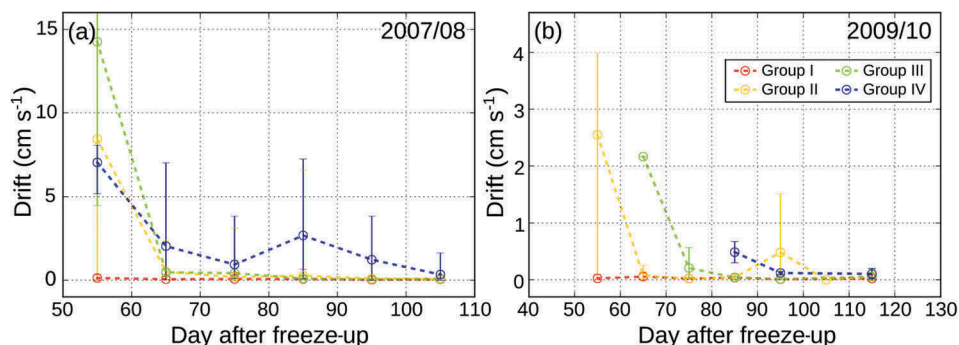
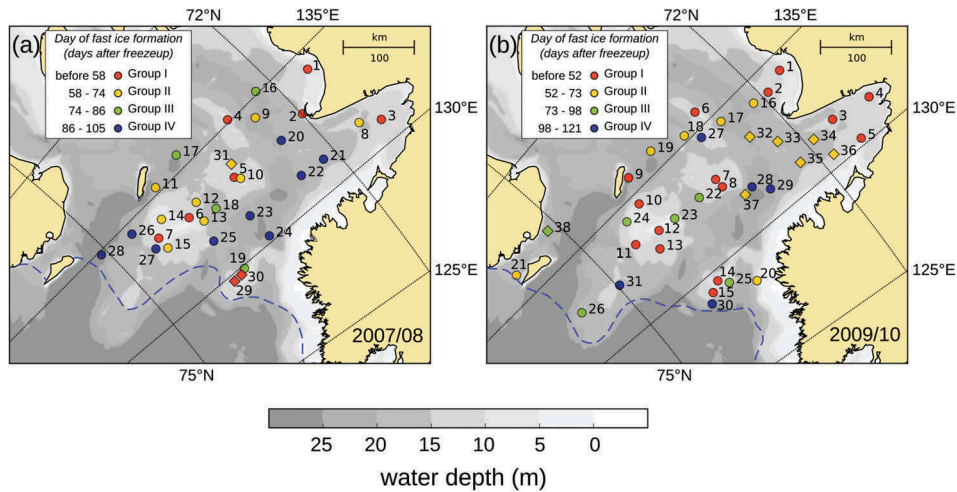
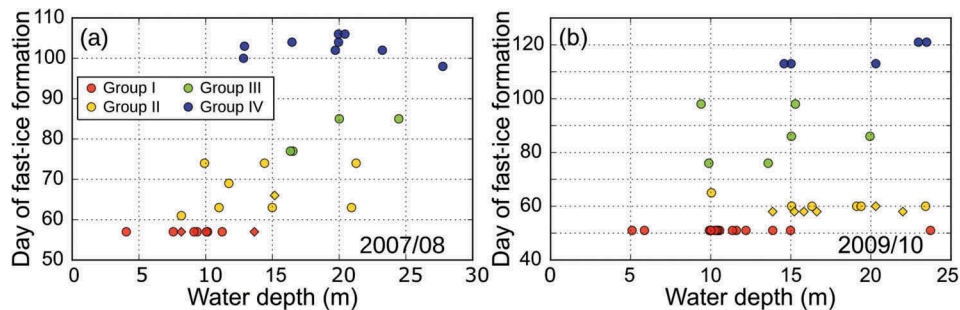


Figure 4. Time series of 10-day mean drift speed for Groups I–IV. The error bars show range of drift for each time step.



**Figure 5.** Final location of the tracked features: (a) 2007/08, (b) 2009/10. Dot colour corresponds to a feature's fast-ice group (Group I-IV). The days of fast-ice formation are given in days after freeze-up. The dashed blue line shows the position of fast-ice edge on (a) 23 January 2008 and (b) 16 February 2010, taken from GDSIDB operational sea-ice charts (WMO 2016).



**Figure 6.** Scatter plot of water depth at the final ice feature location against the day of fast-ice formation. Dot colour corresponds to a feature's fast-ice group.

out events affected one feature in the fast-ice interior (feature 31) and two features closer to fast-ice edge (feature 29, 30). In contrast, an extensive break-out event took place in 2009/10 (Fig. 1), reflected in five neighbouring features (feature 32–36) detaching north of Buor-Khaya Bight (Fig. 5b).

### Sea-ice ridging

Histograms and flight tracks of surveys performed in 2008 and 2012 are shown in Fig. 7. The histogram of ice thickness measurements for flights made in 2012 is characterized by bimodal distribution. The most frequently occurring ice thickness, the mode of the distribution, represents level ice thickness. An analysis of SAR images obtained in the winter of 2012 showed that fast-ice areas characterized by 0.6 m modal thickness are associated to zones that were formed later, while thicker ice (modal thickness around 1.2 m) were formed earlier in the season. The fraction of dynamically deformed ice is represented by the length and the shape of the tail of the thickness distribution. For 2012, the tail is rather narrow, pointing to the absence of deformation in the survey area. The maximal keel

depth of few identified sea-ice ridges did not exceed 9 m which is significantly smaller than the water depth at their location. In contrast, measurements that were made close to the fast-ice edge in 2008 show large differences in mean (2.8 m) and modal thickness (1.4 m) and the histogram characterized by a distinct tail. The profile taken on 29 April 2008 (Fig. 8) shows a deep ice ridge with an estimated ice draft of 18 m. The ridge is located in the fast-ice zone in the vicinity of fast-ice edge where the water depth does not exceed 20 m and therefore is potentially grounded. Deep ice keels were also observed by IPS in the pack ice area in fall 2013 (Fig. 9) While the minimum (level ice) observed sea-ice draft in November–December does not exceed 1 m, the maximal draft (ridge keels) values reach up to 10–18 m.

### Discussion

Investigating the development of fast ice by means of high resolution satellite and observational data we described the formation of fast-ice cover in winter 2007/08 and 2009/10. In both seasons, the fast-ice cover was mainly formed from the drifting sea ice produced during freeze-up in the region (most of the

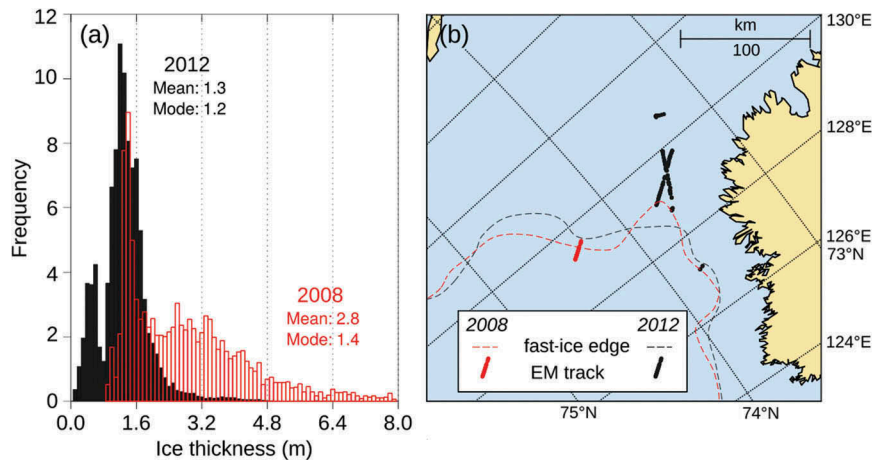


**Figure 7.** (a) The ice thickness distribution measured in April 2008 and 2012. (b) The EM measurements taken along tracks close to the fast-ice edge. The dashed lines show the fast-ice edge on 7 May 2008 (red) and 17 April 2012 (black).

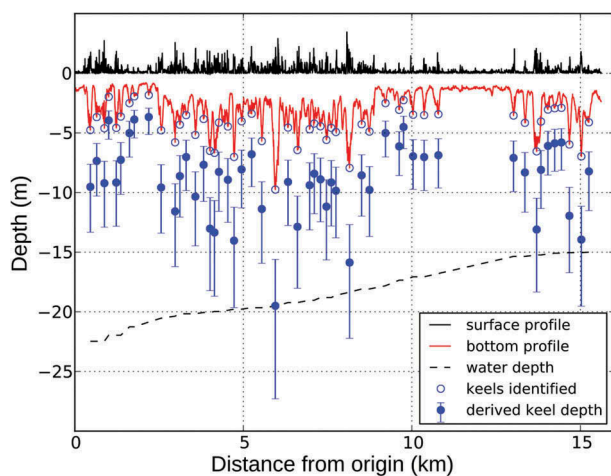


**Figure 8.** The sea-ice surface and bottom topography profiles measured on 29 April 2008. The identified keels depths and derived keel depths are shown in circles. The error bars corresponds to possible ranges of estimated keel depths resulted from different identified-to-derived keel depths ratio found in the literature.

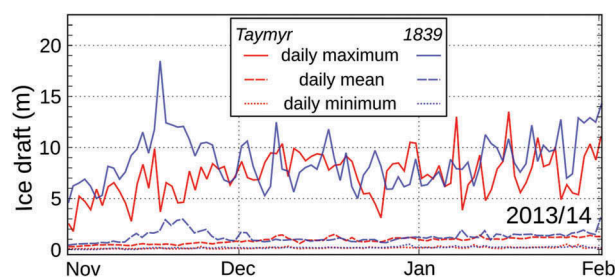


**Figure 9.** Ice draft data obtained by the two IPS systems, Taymyr (77.25°N/116°E) and 1839 (76°N/126°E). The solid, dashed and dotted lines show daily maximum, mean and minimum draft thickness recorded.

features were tracked from the beginning until the end of investigation). Different sea-ice and wind conditions during the two seasons led to typically rapid development of the maximum winter fast-ice extent

in 2007/08 and a more prolonged development period in 2009/10, which included a partial breakout and temporary decrease of fast-ice extent. In 2007/08 the persistent offshore wind facilitated gradual concretion of the thickening pack ice. The offshore grounded features restricted sea-ice motion away from the region which resulted in fast-ice consolidation over a large area. The stronger wind in 2009/10 led to higher sea-ice deformation and opening of a lead east of the Lena Delta where new ice was produced. Consequently, fast-ice cover was formed from thinner sea ice and broke out under a strong wind action. Nevertheless, there was a common pattern of fast-ice formation. First, the formation of extensive fast-ice cover started with development of offshore stationary ice zones (Group I features). Second, during fast-ice consolidation, areas of moving ice were present between the seaward fast-ice edge and the mainland.

The grounded features formed over shoals with the water depth less than 10 m (taken from the International Bathymetric Chart of the Arctic Ocean [Jakobsson et al. 2012]) and re-occurred in both years. The presence of grounded ice at the shoals (stamukhi) is a well-known phenomenon in the Laptev Sea (Gorbunov et al. 2008). The stamukhi were mapped during air reconnaissance flights in 1960-90s. However, there was no information on the timing of their formation, since the flights were done mainly during the navigation period (March–October). According to our investigation, the grounded features formed less than two months after the freeze-up, when the sea-ice thermodynamic thickness (calculated from freezing degree days, using Lebedev 1938 ice growth model) did not exceed 50 cm.

According to IPS data, newly formed ice of less than 50-cm thickness is capable of forming ice keels deep enough to become grounded. The data indicate

that as early as November–December first-year ice had an ice keel of 10 to 18 m (Fig. 9). The bathymetry of the Laptev Sea is based on 5-m contour charts (Jakobsson et al. 2012), which could result in a smoother representation of underwater relief. Taking into account that the International Bathymetric Chart of the Arctic Ocean water depth over the shoals is 5–15 m, an inaccuracy of a few metres can explain grounding of not strongly deformed sea ice. This could explain absence of deformation features on satellite imagery in the region, as reported by Eicken et al. (2005).

The grounded ice features play a key role in fast-ice formation. First, they become an obstacle for the export of sea-ice offshore. Although in 2007/08 the main wind direction was offshore, there was almost no northward transport of ice out of the area south of the grounded features. The only features that exited the study area were those that were initially located between the Lena Delta and the chain of shoals near the longitude of 133°E. Second, grounded features serve as anchors for the surrounding pack ice. As a result, fast ice develops around the grounded features. Therefore, the fast-ice expansion takes place not only in an offshore direction by attachment of pack ice to the seaward fast-ice edge, but also from the central part of the region.

Since grounded fast ice over the shoal areas forms ahead of the main fast-ice edge, sometimes areas of mobile ice can be found between the seaward fast-ice edge and the land. Formation of mobile ice patches within the fast-ice cover can also occur in regions where there is a possibility of ice stabilization offshore. Moving ice can be trapped between the mainland and ice ridges along the Alaskan shore or between chain of islands and the mainland in the Kara Sea. The presence of mobile ice within fast-ice cover has several implications. Because of low drift speed, small-scale and the presence of fast ice seaward, operational sea-ice charts might misclassify these areas of mobile ice as part of fast-ice cover. However, unlike within a consolidated fast-ice cover, formation of leads and deformed ice is likely in these areas. This can endanger local communities in Alaska (John et al. 2004), and to a lesser extent in the Siberian Arctic, in which people hunt and travel on fast ice. The presence of open water can also benefit marine mammals that require active openings. The numerical models that simulate seasonal and interannual variability of fast-ice use drift speed to define fast ice (Wang et al. 2014). Mobile ice behind the fast-ice edge might result in higher mean drift velocities, which might affect simulated timing and spatial pattern of fast-ice formation.

The grounded features also provide additional stability for the fast-ice cover later in the season. During the break-out event in 2009/10, fast ice over the

shoals remained stationary, while the ice located over the deeper area east of the Lena Delta broke out. This area was also covered with fast ice relatively late in 2007/08, although no distinct break-out took place (Fig. 5). A similar pattern of spatial fast-ice development in two seasons with different atmospheric forcing confirms that the location of the grounded ice pre-defines winter fast-ice extent (Selyuzhenok et al. 2015).

While re-occurrence of the grounded ice features in the central part of the south-eastern Laptev Sea constrains the position of the fast-ice edge in this region and reduces interannual variability in fast-ice extent, the deep ridges might be responsible for local variations in the shape of fast-ice edge in winter. The ridges pin fast ice at their location and serve as stabilizing points. Such ridges were detected at the fast-ice edge by the EM method in April 2008. However, the origin of the ridges is not clear: they could form through a deformation within the pack or as a result of deformation at the fast-ice edge. The data indicate that ice ridges with deep keels can be brought to the south-eastern area from the north of the Laptev Sea. Numerical studies confirm that grounding is one of the key mechanisms of fast-ice formation in the Laptev Sea. Parameterization of grounded ridges contributes to more realistic simulations of the seasonal fast-ice cycle (Lemieux et al. 2015; Lemieux et al. 2016).

## Conclusion

A detailed examination of SAR-based ice drift in the winters of 2007/08 and 2009/10 showed that grounding is a key mechanism of fast-ice formation in the south-eastern Laptev Sea. The grounded ice features (stamukhi) are formed offshore prior to fast-ice expansion. These features become an obstacle restricting the motion of the surrounding ice before it becomes stationary and serve as stabilizing points during fast-ice formation. The re-occurrence of grounded features reduces interannual variability in fast-ice extent in the region. Small interannual variations in fast-ice edge position can be explained by formation of deep ridges further offshore. However, there is lack of observational data confirming this hypothesis. The formation of grounded ridges in the vicinity of fast-ice edge and their role in fast-ice formation in the Laptev Sea requires further investigation.

## Acknowledgements

The IPS data were obtained within the framework of Laptev Sea System, a Russian–German cooperative research project. The study reported here was carried out as part of the same project and the project Quantifying Rapid Climate Change in

the Arctic: Regional Feedbacks and Large-Scale Impacts, funded by the German Federal Ministry of Education and Research (grant no. 03F0777A). VS acknowledges support of Russian Science Foundation project no. 17-17-01151. Constructive comments by Jean-François Lemieux and an anonymous reviewer improved the manuscript.

## Disclosure statement

No potential conflict of interest was reported by the authors.

## Funding

This work was supported by the Bundesministerium für Bildung und Forschung (03F0777A); Russian Science Foundation (17-17-01151).

## ORCID

Valeria Selyuzhenok  <http://orcid.org/0000-0001-9388-5706>

## References

- Castellani G., Gerdes R., Losch M. & Lüpkes C. 2015. Impact of sea-ice bottom topography on the Ekman pumping. In G. Lohmann et al. (eds.): *Towards an interdisciplinary approach in earth system science*. Pp. 139–148. Dordrecht: Springer International Publishing.
- Divine D.V., Korsnes R. & Makshtas A.P. 2004. Temporal and spatial variation of shore-fast ice in the Kara Sea. *Continental Shelf Research* 24, 1717–1736.
- Divine D.V., Korsnes R., Makshtas A.P., Godtlielsen F. & Svendsen H. 2005. Atmospheric-driven state transfer of shore-fast ice in the northeastern Kara Sea. *Journal of Geophysical Research—Oceans* 110, C09013, doi: [10.1029/2004JC002706](https://doi.org/10.1029/2004JC002706)
- Dmitrenko I., Kirillov S., Eicken H. & Markova N. 2005. Wind-driven summer surface hydrography of the eastern Siberian shelf. *Geophysical Research Letters* 32, L14613, doi: [10.1029/2005GL023022](https://doi.org/10.1029/2005GL023022)
- Eicken H., Dmitrenko I., Tyshko K., Darovskikh A., Dierking W., Blahak U., Groves J. & Kassens H. 2005. Zonation of the Laptev Sea landfast ice cover and its importance in a frozen estuary. *Global and Planetary Change* 48, 55–83.
- Gorbunov J.A., Losev S.M. & Dymant L.N. 2008. Stamuhi morja Laptevyh. (Stamukhas of the Laptev Sea.) *Problemy Arktiki i Antarktiki* 2, 111–116.
- Haas C. 2004. EM ice thickness measurements during GreenICE 2004 field campaign. GreenICE deliverable D11. Data set. Bremerhaven: World Data Center Pangaea, Alfred Wegener Institute
- Haas C., Lobach J., Hendricks S., Rabenstein L. & Pfaffling A. 2009. Helicopter-borne measurements of sea ice thickness, using a small and lightweight, digital EM system. *Journal of Applied Geophysics* 67, 234–241.
- Hendricks S. 2009. *Validation of altimetric sea-ice thickness measurements with a helicopter based electromagnetic induction method*. PhD thesis, University of Bremen.
- Hendricks S., Hunkeler P., Krumpfen T., Rabenstein L., Eicken H. & Mahoney A. 2014. Sea ice thickness surveying with airborne electromagnetics-grounded ridges and ice shear zones near Barrow, Alaska. Paper presented at the OTC Arctic Technology Conference. Offshore Technology Conference, 10–12 February, Houston, TX.
- Hibler W.D. 1972. Removal of aircraft altitude variation from laser profiles of the Arctic ice pack. *Journal of Geophysical Research* 77, 7190–7195.
- Hibler W.D. 1975. Characterization of cold-regions terrain using airborne laser profilometry. *Journal of Glaciology* 15, 329–347.
- Hughes N.E., Wilkinson J.P. & Wadhams P. 2011. Multi-satellite sensor analysis of fast-ice development in the Norske Øer Ice Barrier, northeast Greenland. *Annals of Glaciology* 52, 151–160.
- Itkin P., Losch M. & Gerdes R. 2015. Landfast ice affects the stability of the Arctic halocline: evidence from a numerical model. *Journal of Geophysical Research—Oceans* 120, 2622–2635.
- Jakobsson M., Mayer L., Coakley B., Dowdeswell J.A., Forbes S., Fridman B., Hodnesdal H., Noormets R., Pedersen R., Rebesco M. & Schenke H.W. 2012. The International Bathymetric Chart of the Arctic Ocean (IBCAO) version 3.0. *Geophysical Research Letters* 39, L12609, doi: [10.1029/2012GL052219](https://doi.org/10.1029/2012GL052219)
- John C., Huntington H.P., Brewster K., Eicken H., Norton D.W. & Glenn R. 2004. Observations on shorefast ice dynamics in Arctic Alaska and the responses of the Inupiat hunting community. *Arctic* 57, 363–374.
- Karklin V.P., Karelin I.D., Julin A.V. & Usol'ceva E.A. 2013. Osobennosti formirovaniya pripaja v more Laptevyh. (Peculiarities of landfast ice formation in the Laptev Sea.) *Problemy Arktiki i Antarktiki* 3, 5–13.
- Lebedev V.V. 1938. The dependence between growth of ice in Arctic rivers and seas and negative air temperature. *Problemy Arktiki* 5, 9–25.
- Lemieux J.F., Dupont F., Blain P., Roy F., Smith G.C. & Flato G.M. 2016. Improving the simulation of landfast ice by combining tensile strength and a parameterization for grounded ridges. *Journal of Geophysical Research—Oceans* 121, 7354–7368.
- Lemieux J.F., Tremblay L.B., Dupont F., Plante M., Smith G.C. & Dumont D. 2015. A basal stress parameterization for modeling landfast ice. *Journal of Geophysical Research—Oceans* 120, 3157–3173.
- Mahoney A., Eicken H., Gaylord A.G. & Shapiro L. 2007. Alaska landfast sea ice: links with bathymetry and atmospheric circulation. *Journal of Geophysical Research—Oceans* 112, C02001, doi: [10.1029/2006JC003559](https://doi.org/10.1029/2006JC003559)
- Markus T., Stroeve J.C. & Miller J. 2009. Recent changes in Arctic sea ice melt onset, freezeup, and melt season length. *Journal of Geophysical Research—Oceans* 114, C12024, doi: [10.1029/2009JC005436](https://doi.org/10.1029/2009JC005436)
- Melling H., Johnston P.A. & Riedel D.A. 1995. Measurements of the underside topography of sea ice by moored subsea sonar. *Journal of Atmospheric and Oceanic Technology* 13, 589–602.
- Olasen E. 2016. A dynamical model of Kara Sea land-fast ice. *Journal of Geophysical Research—Oceans* 121, 3141–3158.
- Pfaffhuber A.A., Hendricks S. & Kvistedal Y.A. 2012. Progressing from 1D to 2D and 3D near-surface airborne electromagnetic mapping with a multisensor, airborne sea-ice explorer. *Geophysics* 77, WB109–WB117.
- Pfaffling A., Haas C. & Reid J.E. 2007. Direct helicopter EM—sea-ice thickness inversion assessed with synthetic and field data. *Geophysics* 72, F127–F137.
- Pickart R.S., Spall M.A., Moore G. W.K., Weingartner T.J., Woodgate R.A., Aagaard K. & Shimada K. 2011. Upwelling in the Alaskan Beaufort Sea: atmospheric

- forcing and local versus non-local response. *Progress in Oceanography* 88, 78–100.
- Proshutinsky A., Ashik I., Häkkinen S., Hunke E., Krishfield R., Maltrud M., Maslowski. W. & Zhang J. 2007. Sea level variability in the Arctic Ocean from AOMIP models. *Journal of Geophysical Research—Oceans* 112, C04S08, doi: [10.1029/2006JC003916](https://doi.org/10.1029/2006JC003916).
- Reid J.E., Vrbancich J. & Worby A.P. 2003. A comparison of shipborne and airborne electromagnetic methods for Antarctic sea ice thickness measurements. *Exploration Geophysics* 34, 46–50.
- Reimnitz E., Dethleff D. & Nürnberg D. 1994. Contrasts in Arctic shelf sea-ice regimes and some implications: beaufort Sea versus Laptev Sea. *Marine Geology* 119, 215–225.
- Selyuzhenok V., Krumpfen T., Mahoney A., Janout M. & Gerdes R. 2015. Seasonal and interannual variability of fast ice extent in the southeastern Laptev Sea between 1999 and 2013. *Journal of Geophysical Research—Oceans* 120, 7791–7806.
- Timokhov L.A. 1994. Regional characteristics of the Laptev and the East Siberian seas: climate, topography, ice phases, thermohaline regime, circulation. *Berichte zur Polarforschung* 144, 15–31.
- Wadhams P. & Davy T. 1986. On the spacing and draft distributions for pressure ridge keels. *Journal of Geophysical Research—Oceans* 91, 10697–10708.
- Wang J., Mizobata K., Bai X., Hu H., Jin M., Yu Y., Ikeda M., Johnson W., Perie W. & Fujisaki A. 2014. A modeling study of coastal circulation and landfast ice in the near-shore Beaufort and Chukchi seas using CIOM. *Journal of Geophysical Research—Oceans* 119, 3285–3312.
- WMO (World Meteorological Organization) 2016. Global digital sea ice data bank project. WDCB (World Data Center – B “Oceanography”) Sea Ice. Arctic and Antarctic Research Institute 7-days period generalized ice charts for the Russian Arctic and seasonal ice cover seas and the Greenland Sea for 1998-2013. Accessed on the internet at <http://wdc.aari.ru/datasets/d0004/> on 23 September 2016.